J Membrane Biol (2009) 231:35–46
DOI 10.1007/s00232-009-9202-4

Optical Coherence Tomography Phase Measurement of Transient Changes in Squid Giant Axons During Activity

Taner Akkin · David Landowne · Aarthi Sivaprakasam

Received: 10 June 2009 / Accepted: 10 September 2009 / Published online: 6 October 2009

Abstract Noncontact optical measurements reveal that transient changes in squid giant axons are associated with action potential propagation and altered under different environmental (i.e., temperature) and physiological (i.e., ionic concentrations) conditions. Using a spectral-domain optical coherence tomography system, which produces real-time cross-sectional images of the axon in a nerve chamber, axonal surfaces along a depth profile are monitored. Differential phase analyses show transient changes around the membrane on a millisecond timescale, and the response is coincident with the arrival of the action potential at the optical measurement area. Cooling the axon slows the electrical and optical responses and increases the magnitude of the transient signals. Increasing the NaCl concentration bathing the axon, whose diameter is decreased in the hypertonic solution, results in significantly larger transient signals during action potential propagation. While monophasic and biphasic behaviors are observed, biphasic behavior dominates the results. The initial phase detected was constant for a single location but alternated for different locations; therefore, these transient signals acquired around the membrane appear to have local characteristics.

T. Akkin (✉) · A. Sivaprakasam
Department of Biomedical Engineering,
University of Minnesota, 7-105 Hasselmo Hall,
312 Church St. SE, Minneapolis, MN 55455, USA
e-mail: akkin@umn.edu

D. Landowne
Department of Physiology and Biophysics, University of Miami,
PO Box 016430, Miami, FL 33101, USA

Keywords Action potential · Optical coherence tomography · Phase measurement · Functional neural imaging

Introduction

The use of optical instrumentation to study neural activity dates to the late 1940s. Since the optical imaging techniques are able to provide high spatial and temporal resolutions, they have been utilized widely for structural and functional investigations. The indicators of neural activity that can be detected optically include absorption, fluorescence, optical rotation, retardance, scattering and volume changes (Cohen 1973). Hill and Keynes (1949) reported an increase in scattering followed by a decrease due to stimulation of crab nerve. Cohen et al. (1968, 1969, 1970) demonstrated light scattering and birefringence changes due to action potentials (APs) in squid giant axon, crab nerve and eel electric organ. Changes in fluorescence, light scattering and birefringence during excitation of crab and lobster nerves were reported by Tasaki et al. (1968). Using olfactory nerve of pike, von Muralt (1975) reported that the birefringence changes can be recorded without averaging. These signals are associated with neural activity (i.e., AP propagation) and are likely to be related to each other. For example, the retardance (birefringence multiplied by thickness) and scattering changes can be a result of one or more of the following factors: conformational changes in the membrane channels, influx and outflux of ions during AP propagation and mechanical changes occurring on the axonal surfaces.

There have been a number of instances where mechanical changes occurring during AP propagation have been measured. Using an optical method, Hill (1950)

reported a cumulative increase in the radius of a cuttlefish axon of about 0.1 μm for 10,000 impulses. At a high rate of stimulation an initial transient shrinkage preceding this cumulative swelling was also reported. Bryant and Tobias (1955) demonstrated a shortening in length of crab and lobster nerves due to stimulation. Using a laser interferometer and gold particles on a crayfish giant axon, Hill et al. (1977) reported a 1.8-nm contraction of the axon followed by a slow swelling. Iwasa and Tasaki (1980) used a fiber-based sensor and gold particles on squid giant axon to report a 0.5-nm swelling of the axon surface over a 1-ms period. Rapid mechanical changes in garfish olfactory nerve were measured using a piezoceramic bender. Concurrent with the AP, swelling of nerve fibers as well as shortening in length were reported (Tasaki et al. 1989; Tasaki and Byrne, 1990). Also, an optical lever placed on a lobster nerve and a knife edge was used to report a swelling of <1 nm (Yao et al. 2003). Akkin et al. (2004) demonstrated noncontact, depth-resolved optical measurement of transient structural changes using differential phase interferometry and reported surface and subsurface displacements (in swelling and shrinkage directions) that were ~1 nm in magnitude and ~1 ms in duration using crayfish nerve bundles. Another phase-sensitive interferometric technique was utilized for measurement of lobster nerve surface swelling, which was reported to be ~5 nm in magnitude and ~10 ms in duration (Fang-Yen et al. 2004). Spectral-domain optical coherence tomography (SD-OCT) was reported for the measurement, which showed 0.5–2.5 nm transient changes within crayfish and lobster nerve bundles during AP propagation (Akkin et al. 2007). Moreover, Kim et al. (2007) demonstrated a rapid (<2 ms) increase in the thickness of mouse neurohypophysis lobe of about 5–10 nm using atomic force microscopy and reported that AP-related light-scattering signals are associated with changes in terminal volume. The result is encouraging for probing the mammalian nerve terminals during activity with SD-OCT, which has advantages due to its noncontact and depth-resolved nature, avoiding unintentional damage to tissue. The exact nature of the transient structural changes occurring on neural surfaces is not yet conclusive. The magnitude, duration and profile of the changes, as well as the physiological phenomena leading to it, need to be understood for simple and complex neural tissues.

We present transient signals acquired from squid giant axons during AP propagation at room and cold temperatures and in normal and hypertonic solutions. SD-OCT, which detects intensity and phase of interference along a full depth profile, is utilized for noncontact, reflection-mode measurements. In the experiments, cross-sectional images of the axon in a nerve chamber are displayed in real time. Then, axonal surfaces along a depth profile are probed simultaneously for functional changes. The transient signals are detected by differential phase measurement, which is then converted to optical path length change. The system yields subnanometer axial resolution and submillisecond temporal resolution for the measurement. An earlier report of our findings has appeared in abstract form (Sivaprakasam et al. 2008).

Materials and Methods

Description of Optical and Electrical Setups

OCT uses the low temporal coherence of a broadband light source to noninvasively construct cross-sectional images of biological tissue with a few micrometer axial resolution up to a depth of a few millimeters (Huang et al., 1991). In contrast to time-domain OCT, SD-OCT does not require mechanical scanning of the reference mirror of a Michelson interferometer along the axial direction. Instead, it uses a spectrometer to capture interference of back-scattered light from all depth points simultaneously (Fercher et al., 1995; Hausler & Lindner, 1998; Wojtkowski et al., 2002), which results in improved imaging speed (Nassif et al., 2004) and phase stability (White et al., 2003; Choma et al., 2005; Joo et al., 2005). A Fourier transform algorithm relates spectral modulations to depth information. Figure 1 shows a schematic of an SD-OCT system together with a nerve chamber used in the sample arm.

Two broadband superluminescent diodes were combined to improve the axial resolution (Δz). The center wavelength (λ_o) and half-power bandwidth ($\Delta\lambda$) of the combined source were 835 and 75 nm, respectively. Correspondingly, an axial resolution of 5.9 μm in air (~4.3 μm in neural tissue) was obtained. The spectrometer in the detection path consists of a custom-built device containing a 75-mm achromatic collimator, 1,200 lines/mm transmission grating (Wasatch Photonics, Logan, UT) and a 100-mm achromatic focusing lens. The optical spectrum was captured by a line scan CCD camera (Basler Vision Technologies, Ahrensberg, Germany) containing a linear array of 2,048 pixels, each measuring 10 × 10 μm.

In the sample path, a 25-mm achromatic lens focused the incoming collimated light (2.4 mm in diameter) with an effective numerical aperture of 0.048. This configuration results in a lateral resolution of 21 μm and a Rayleigh range of 423.5 μm, theoretically. The optical power on the sample did not exceed 1 mW. Three other detectors and the Wollaston prism in the sample path enable recordings of, although not reported here, cross-polarized light intensities in reflection (photodetector D2) and transmission (photodetector D1 placed after an analyzer) geometries; and the

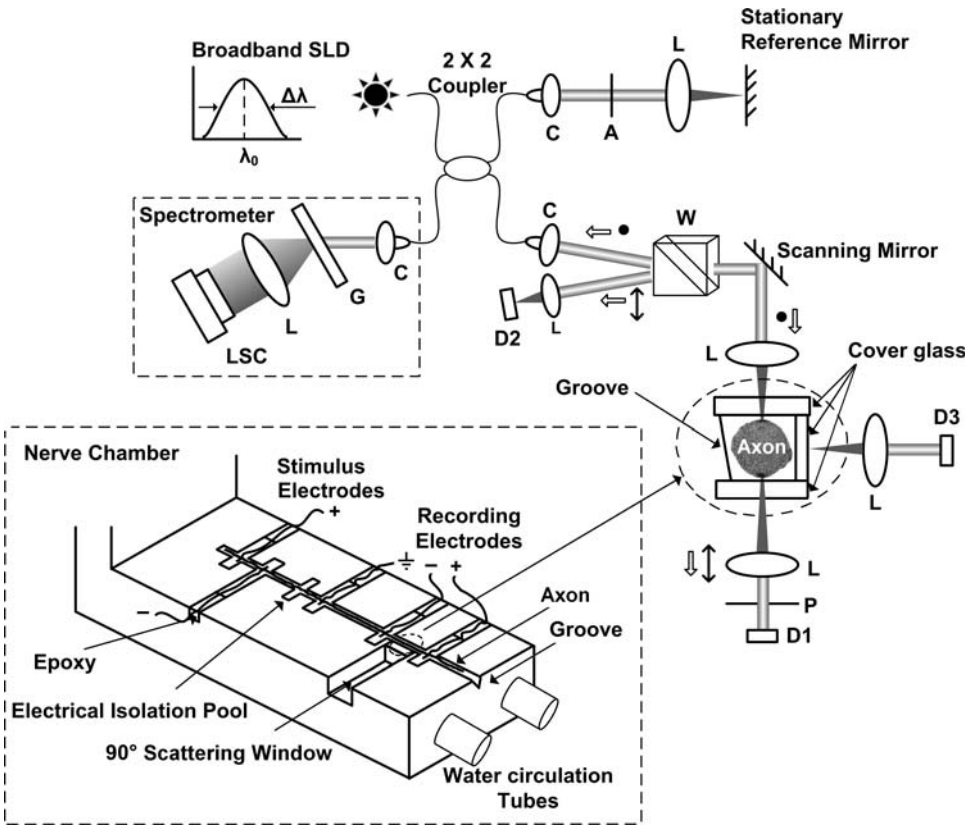

Fig. 1 Schematic of an SD-OCT system and a nerve chamber employed in the sample arm. By scanning the beam over an axon laterally, an axonal cross section is imaged; however, the beam was stationary during the actual recording. Water circulation through the tubes (below the groove) varies the temperature. AP is recorded differentially using platinum wires attached to the chamber. *A* attenuator, *C* light collimator, *D1–D3* detectors for cross-polarized and scattering signals (not reported), *G* transmission grating, *L* lens, *LSC* line scan camera, *P* polarizer, *SLD* superluminescent diode (λ_o 835 nm, $\Delta\lambda$ 75 nm); W, Wollaston prism

third photodetector (D3) can be utilized for scattering measurement.

The nerve chamber was made of Plexiglas with platinum electrodes fixed to the chamber with epoxy to stimulate the axon and to record the electrical AP differentially. A 2-mm-thick cover glass was fixed on top of the chamber in the optical recording zone to provide a glass–saline (glass–seawater) interface, which would serve as a reference for measuring transient structural changes. The electrical signal is the difference in potential between two platinum wires, 6 mm apart, on either side of this optical window. The axon was placed in the groove (1 mm wide, 1 mm deep), and the chamber was oriented with the long axis of the axon at 45° with respect to the polarization direction of the incoming light. The chamber walls contained tubes through which ice water (or room-temperature water) was circulated to vary the axon temperature between experiments.

The experiments were performed using fresh live squids (*Loligo pealeii*) at Marine Biological Laboratory (Woods Hole, MA). Due to its large size, isolation of a single squid axon was relatively easy. The giant axons were extracted under a dissection microscope and cleaned by removing the small fibers around the axon. The axon was kept immersed in filtered Woods Hole seawater during and after dissection. The ends of the axon were tied with sutures and placed in the groove of the nerve chamber containing seawater. Petroleum jelly was used to isolate the recording and stimulating electrodes from each other. Cover glasses were placed on the exposed parts of the axon to prevent them from drying out. An isolated pulse stimulator (model 2100; A-M Systems, Sequim, WA) was used to apply 50-μs duration electrical current pulses of varying amplitudes to the axon. The externally recorded AP was amplified by an AC differential amplifier (model 1800, A-M Systems) with low- and high-cutoff frequencies set to 10 Hz and 10 kHz, respectively. The APs were displayed on an oscilloscope to monitor the functioning of the axon. Axons which exhibited activity for a stimulus amplitude of <1 mA were considered functional. The electrical and optical signals were recorded simultaneously by using data-acquisition cards (models PCI-6110 and PCI-1428; National Instruments, Austin, TX).

The optical technique was able to image the squid giant axon in the nerve chamber with high resolution. Then, the transient structural changes associated with single AP propagation were probed along an axial line, including the top and bottom surfaces of the axon, simultaneously. In addition to its advantageous size, the squid giant axon is unmyelinated. Its microstructure is relatively simpler than the nerve bundles containing populations of different axons. Therefore, the squid giant axon model was an ideal

choice for studying the AP-related transient signals reported here.

Optical Measurement

The spectrometer in the detection arm measures the spectral intensity of the source, the spectral intensity due to interference between the sample and reference signals and the spectral intensity due to autocorrelation caused by mutual interference of light back-scattered from the sample. The latter is assumed to be negligible when compared to the strong reference amplitude. Since spatial information $S(z)$ is encoded in the modulation frequency of the spectrum $S(k)$, the optical path length difference between a sample surface and the reference mirror controls the frequency of the corresponding spectral modulation. The back-scattering amplitude can be deduced by inverse Fourier transform of the spectral intensity $S(k)$. To reduce the amplitude of sidebands in the coherence function, the nongaussian-shaped source spectrum can be converted to a gaussian spectrum by spectral shaping (Tripathi et al. 2002). The signal in the sample and reference arms encounters a dispersion mismatch when there are varying amounts of dispersive media like optical fiber or glass. We compensated for the dispersion mismatch in software (Cense et al. 2004). After processing, the intensity of the resulting complex signal $S(z)$ provides a reflectivity image that shows tissue microstructure with appropriate lateral scanning of the beam over the sample.

The phase $\phi(z)$ is calculated by a four-quadrant inverse tangent of imaginary and real parts of the complex function $S(z)$, where $\phi(z)$ lies in the range $-\pi$ to π. The phase information is reported as single-pass optical path length changes (Δp) at all points along a depth profile simultaneously, $\Delta p(z) = (\lambda_0/4\pi)\Delta\varphi(z)$. To verify accuracy, we imaged a chromium step of height 150 nm (not shown) with differential phase measurement of the SD-OCT and confirmed the height with atomic force microscopy. To determine the minimum detectable Δp, interference between the front and back surfaces of a glass slide was monitored without employing the reference arm. Data were collected for 1 s with a temporal resolution of 34 μs. The standard deviation of the measurement ($\sim$0.75 mrad or $\sim$50 pm) was attributed to the noise because there was no path-length change intentionally induced. The phase noise is related to the signal-to-noise ratio (SNR) (Yazdanfar et al. 2005; Park et al. 2005), $<\Delta\varphi^2> \approx 1/(2SNR)$. Since the SNR decrease in tissues due to low reflectivity and motion artifacts can introduce noise into the measurements, averaging may be required to observe subnanometer-scale changes in optical path length for the biological samples.

Results

SD-OCT Appearance of Axon

In order to select a suitable location for functional measurements, we monitored a scanned cross-sectional image of the squid giant axon in the nerve chamber (Fig. 2a).The axon and associated connective tissue appear as a fairly uniform circular cross section. A small branch with some adherent small fibers and connective tissue is visible on the right side of the axon. There was often a suggestion of a difference in texture between the axon and an approximately 20-μm outer sheath of connective tissue, but a clear separation was not always possible. The dark spots on the top and bottom of the axon are due to strong specular reflections. The gray scale in the image is a logarithmic representation of the intensity of light scattered from each position.

The two almost horizontal lines above and below the axon are the glass–saline (seawater) interfaces of the two windows. The windows were tilted to avoid saturating the line scan camera in the detection arm with the specular reflections from these interfaces. Tilting the window considerably resulted in a thicker line, as shown for the lower saline–glass interface. There are also faint images of the axon (cut from the top) and a glass–water interface due to self-interference of light from various parts of the sample apparatus.

Figure 2b shows the amplitude of the back-scattered light intensity from a single depth profile (A-line) in the center of the scan. The A-line is plotted in a linear scale. From the top, the four most prominent peaks are the upper glass–saline interface, the upper and lower surfaces of the axon and the lower saline–glass interface. There was often a suggestion of substructure in the intensity peaks associated with the axon surfaces.

Neural Activity Can Be Detected as a Δp Response

To study functional changes in the axon, modulations of the optical spectrum were recorded for all depths at a single lateral location every 50 μs. Amplitude and phase information at each depth were extracted as described in "Materials and Methods." The difference in the phase of the light from two selected depths was converted to single-pass optical path-length change (Δp) for convenience and plotted as a function of time to demonstrate the change during AP propagation. The results had 5-kHz bandwidth and were obtained at room temperature, in a cold environment and in normal and hypertonic solutions. We performed measurements on 34 squid giant axons. For each axon we obtained data from multiple locations in the optical recording zone. For each location we normally

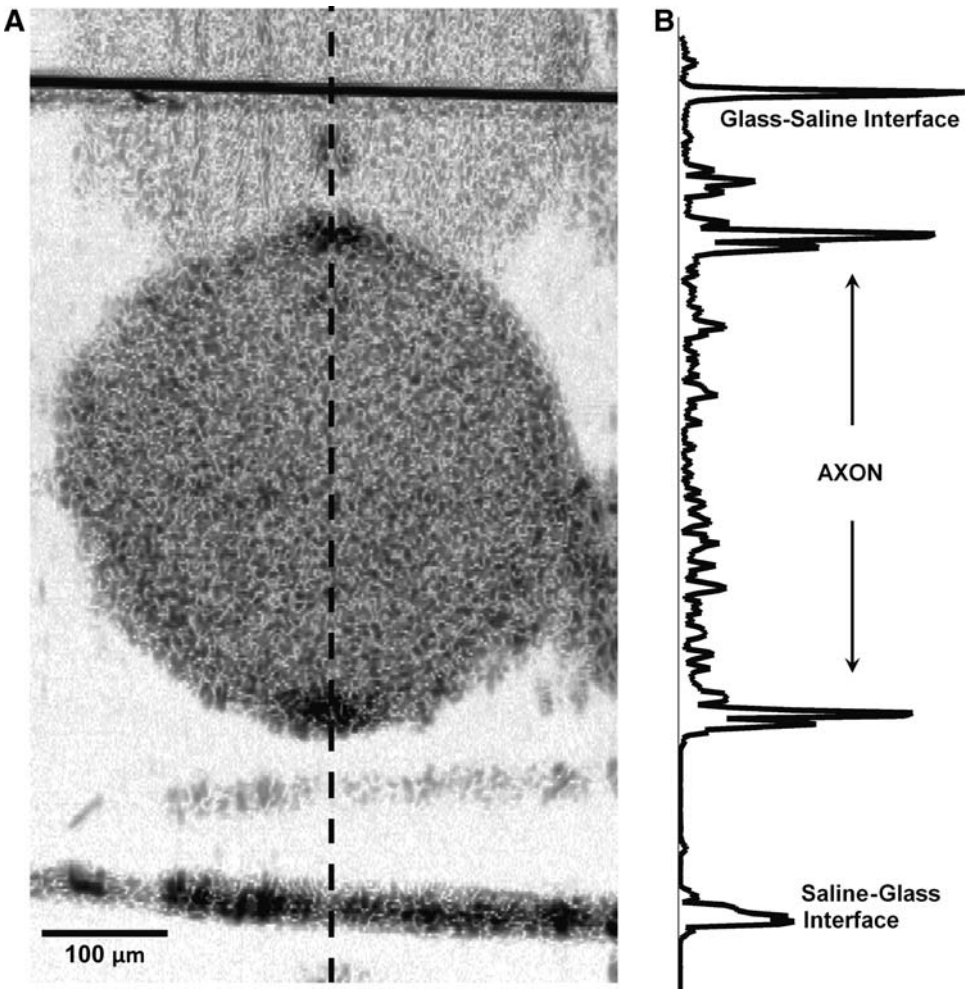

Fig. 2 Cross-sectional image of a squid giant axon (**a**) and intensity of a single depth profile in the center of the scan (*dashed line*) showing the glass–saline interfaces and the axon (**b**)

recorded three trials, each of which contained multiple records, to improve the SNR by averaging. Each record typically consisted of responses to three stimuli, to show the repeatability of the response.

The traces in Fig. 3 show Δp responses during activity and the corresponding AP at room (20–21°C) and cold ($\sim$2°C) temperatures. An upward change in Δp indicates an increase in optical path length between the measurement points (i.e., top and bottom surfaces of the axon), and a downward change represents a decrease. In the room-temperature example (Fig. 3a) we were able to stimulate the axon at high rates. The vertical arrows represent current pulses (300 µA, 50 µs) stimulating the axon. As a result of AP propagation, Δp decreased about 0.3 nm, then increased about 0.7 nm and then returned to its original state in about 5 ms with each AP. The trace represents a biphasic (two directions) signal. Five hundred records were averaged to improve the SNR. The optical signal was roughly synchronous with the electrical AP (extracellular), which is also averaged and plotted for comparison. The overall upward trend in the optical trace may be due to a drift, as opposed to a cumulative effect of stimulation.

Cooling Increases the Magnitude and Duration of the Δp Response

Figure 3b demonstrates transformation of the electrical and optical signals in a cold extracellular environment. Chilled water was circulated through the nerve chamber (below the groove), and the axon's environment was at a temperature of $\sim$2°C. As a result of AP propagation, Δp between the top and bottom surfaces of the axon first decreased and then increased, resulting in a biphasic trend with a return to baseline. The duration of the response is modified according to the duration change in the AP. Compared to room-temperature data (Fig. 3a), the electrical AP is delayed and prolonged in time. The stimulation pulses (600 µA, 50 µs) that are 10 ms apart are indicated by arrows at 8, 18 and 28 ms. For each trace, 250 responses were averaged.

We obtained data at room temperature from 136 trials at various locations on multiple axons. The histogram of the net change in magnitude of the Δp responses, measured peak-to-peak, during AP propagation is plotted in Fig. 4a. The width of the bins is 0.5 nm. For about three-quarters of the 136 trials the change was <1 nm, with the remainder

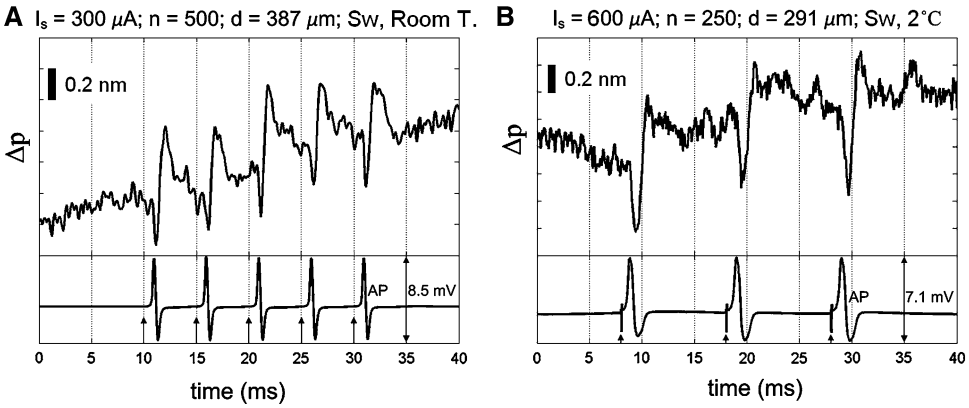

Fig. 3 Optical path-length change (Δp) between top and bottom surfaces of the axons during AP propagation at (**a**) room (~20°C) and (**b**) cold (~2°C) temperatures. The downward and upward changes represent a decrease and an increase in Δp, respectively. The AP is passing the first (–) and second (+) recording electrodes at the positive and negative peaks, respectively. *Small upward arrows* indicate stimulus current pulses of duration 50 μs. I_s stimulus amplitude; *n* number of responses averaged, *d* diameter of the axon, *Sw* seawater

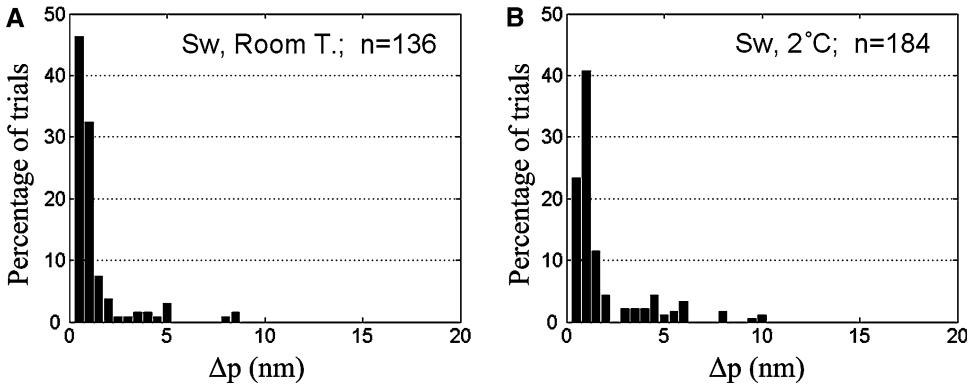

Fig. 4 Histograms of peak-to-peak magnitude of Δp measured between top and bottom surfaces of axons at (**a**) room (~20°C) and (**b**) cold (~2°C) temperatures during AP propagation. *Sw* seawater; *n* total number of trials. Bin size = 0.5 nm

widely scattered up to 8 nm. The mean and standard deviation of the Δp response magnitudes are, respectively, 1.1 and 1.48 nm for all experiments performed at room temperature. For the 108 measurements <1.2 nm, the mean and standard deviation were 0.57 and 0.19 nm, respectively.

Figure 4b shows a histogram of the net change in magnitude of Δp during AP propagation in a cold environment (bin width 0.5 nm). The magnitude of the Δp response was <0.5 nm for about 23% of the 184 trials and 0.5–1 nm for about 40% of the trials. The mean and standard deviation of the Δp response magnitudes are, respectively, 1.65 and 2.01 nm for all experiments performed in a cold environment (~2°C). For the 124 measurements <1.2 nm, the mean and standard deviation were 0.68 and 0.21 nm, respectively. Figure 4b also shows that larger magnitudes are observed occasionally.

Excess NaCl Produces a Larger Signal

We increased the NaCl concentration of the extracellular solution by adding solid NaCl to filtered Woods Hole seawater. This reduced the squid axon diameter. For example, adding 400 mM NaCl to the extracellular solution caused a 360-μm-diameter axon to shrink by 40 μm. After replacing the extracellular solution in the nerve chamber, AP-related changes in Δp were studied in a cold environment (~2°C).

Figure 5 shows the histograms of the Δp response magnitude for axons in seawater containing 200, 400 and 800 mM of additional NaCl. The mean and standard deviation of the Δp response magnitudes are, respectively, 5.29 and 6.04 nm for 200 mM excess NaCl ($n = 41$ trials), 4.86 and 5.76 nm for 400 mM excess NaCl ($n = 51$ trials) and 6.25 and 4.69 nm for 800 mM excess NaCl ($n = 20$ trials). The results are clearly larger than the Δp magnitudes produced in plain seawater. We split these results (Fig. 5a–c) into two parts since the larger magnitudes are separated widely from the main distribution. Although these large signals in the range of 10–20 nm deserve extra attention, we performed gaussian fitting for trials whose Δp response magnitudes do not exceed 8 nm. Figure 5d shows the resulting curves and the data observed in 0.2-nm-wide bins. The mean and standard deviation of these distributions are,

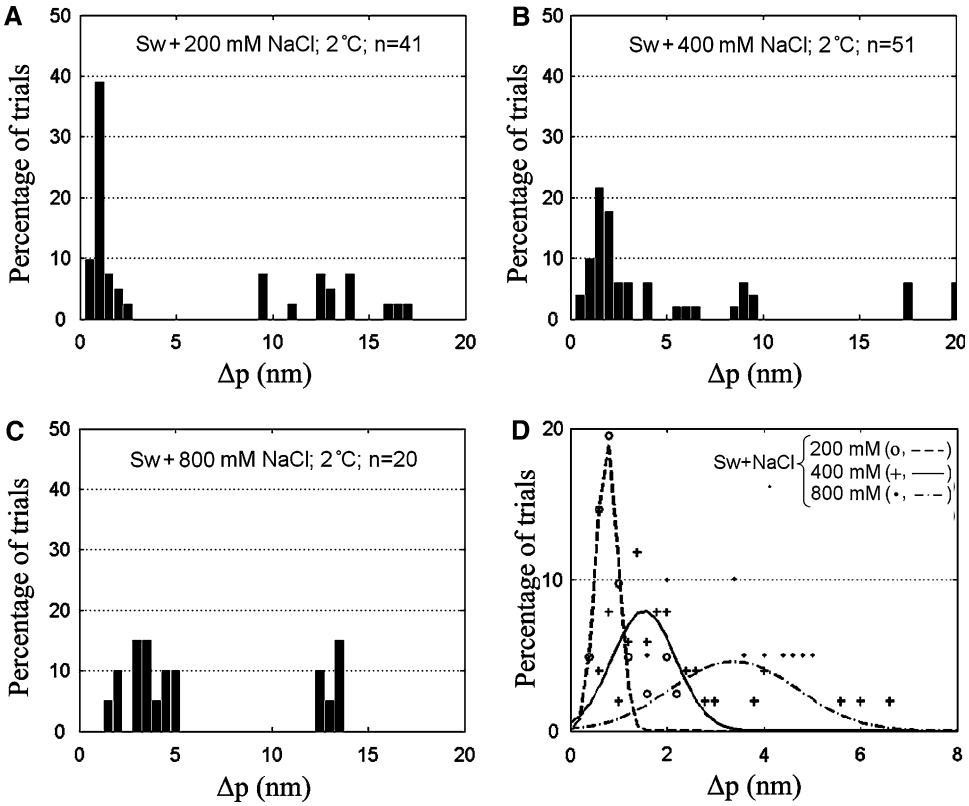

Fig. 5 Histograms of peak-to-peak magnitude of Δp measured between top and bottom surfaces of axons in cold seawater with (**a**) 200 mM, (**b**) 400 mM and (**c**) 800 mM additional NaCl. *Sw* seawater, *n* total number of trials. Bin size = 0.5 nm. Gaussian fitting (- -, —, -.-) for trials whose Δp magnitudes do not exceed 8 nm and the data observed (o, +, •) in 0.2-nm-wide bins are shown in **d**

respectively, 0.77 and 0.22 nm for 200 mM excess NaCl ($n = 26$ trials), 1.53 and 0.65 nm for 400 mM excess NaCl ($n = 39$ trials) and 3.39 and 1.29 nm for 800 mM excess NaCl ($n = 14$ trials). Therefore, the results shown in Fig. 5d suggest that squid giant axons produce larger Δp responses in the presence of increased levels of NaCl in the axon's environment.

Shape and Direction of the Δp Response

There was considerable variability in the shape and direction of the optical signals. Figure 6 shows two examples recorded from axons in cold seawater. The top and bottom Δp traces in Fig. 6a represent optical path-length changes of the top and bottom surfaces of an axon with respect to a reference surface (glass–seawater interface above the axon), respectively. An upward change indicates a decrease, and a downward change indicates an increase in optical path length between a surface and the top reference glass. Figure 6b shows Δp between the top and bottom surfaces of the axon, which does not need the reference surface and is equivalent to the subtraction of the two traces in Fig. 6a. The electrical AP recordings as a result of stimulation pulses (arrows) are also shown. The optical trace shows a 9-nm transient increase in Δp. Since there is no apparent additional phase in the response, we called the transient response "monophasic." Traces in Fig. 6c, d show a more complex pattern. Both downward and upward components are observed, and some of these components are not equally strong for the top and bottom surfaces of the axon (Fig. 6c). The traces for the top and bottom surfaces show changes in opposite directions, though in some cases we also observed that the two surfaces yield change in the same direction. In Fig. 6d, Δp between the axonal surfaces exhibits a "multiphasic" behavior, with an initial decrease in Δp followed by an increase. The response also shows an additional cycle of decrease, which is uncommon.

Biphasic and monophasic behaviors of Δp between the axonal surfaces were counted for experiments performed at room and cold temperatures and for experiments with increased levels of NaCl concentration in cold. About 5% of the responses were multiphasic and were included in the biphasic category. Figure 7a shows the percentages of the biphasic and monophasic responses during AP propagation: 75% of the responses were clearly biphasic at room temperature; the remainder appeared to be monophasic. Biphasic responses with additional NaCl in seawater were even more frequent. As shown, the biphasic response dominated the results for all cases. In addition, in about 15% of the trials we did not see a net difference in Δp above the 0.2-nm noise level.

The results also showed that the initial direction of Δp responses varied. Figure 7b shows the percentage of trials for experiments performed at room and cold temperatures

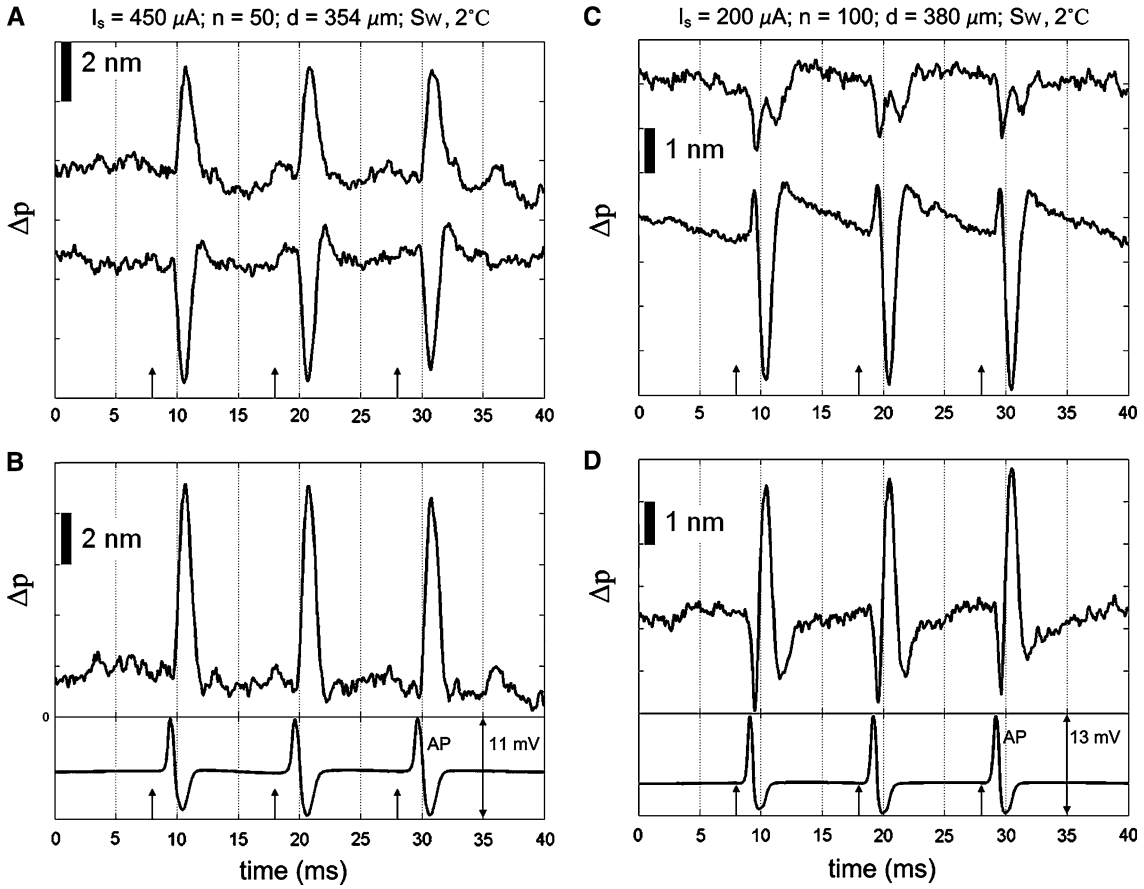

Fig. 6 Monophasic (**a**, **b**) and multiphasic (**c**, **d**) patterns recorded from squid giant axons during AP propagation. *Top* and *bottom traces* in **a** and **c** are acquired from the top and bottom surfaces of the axon with respect to the reference glass. Δ*p* traces in **b** and **d** are measured between the top and bottom surfaces of the axon and are equivalent to the subtraction of the traces in **a** and **c**, respectively. I_s stimulus amplitude, *n* number of responses averaged *d* diameter of the axon, *Sw* seawater

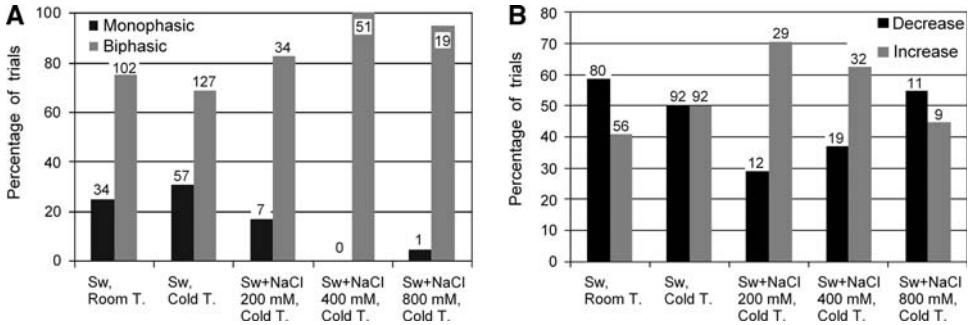

Fig. 7 Comparisons of monophasic and biphasic patterns (**a**) and direction of the initial event (**b**) detected in Δ*p* between top and bottom surfaces of the axons during AP propagation. Number of trials is indicated above the bars

and for experiments with increased levels of NaCl concentration in cold. Both decrease and increase phases in Δ*p* were observed as the first event during AP propagation. When a measurement was repeated without moving the axon, the sign of the Δ*p* response did not change. Responses of both signs were found on the same axon. We could not see a pattern between sign of the response and position along the axon.

Stability of the Response

Figure 8a shows a single and an average of 50 responses with the corresponding AP. A 21-nm peak-to-peak Δ*p* response between the top and bottom surfaces of the axon was obtained at cold temperature with 400 mM NaCl added to the seawater. By accumulating responses to consecutive stimuli, our method may be utilized for studying the

progression of these fast signals. Figure 8b shows the result in a three-dimensional plot. Each trace along the fast time axis is a moving average of 10 records. As shown, the fast response is preserved for the entire 10 s, indicating the stability and repeatability of the measurement. The fast response for a given depth profile was repeatable. In Fig. 8b, the slope along the slow time axis may be due to drift and, therefore, is not conclusive evidence for a cumulative effect.

Discussion

The SD-OCT method clearly shows that the optical signal (Δp response) corresponds to the passage of APs. Both electrical and optical measurements show fast changes at room temperature and relatively slow changes in a cold environment in which the speed of the AP is reduced. Since the optical readout area is between the external electrodes recording AP differentially, the zero-crossing of the electrical signal coincides with the optical signal, as expected. The optical signals, when observed, were all-or-none with the same threshold as the electrical signal. In some runs the interstimulus time within the train was short enough that not all stimuli were effective at producing an AP (data not shown). In these cases the corresponding optical signal was also missing. However, in about 15% of all trials we did not observe a net difference in Δp.

We observed biphasic Δp responses from squid giant axon for the majority of cases, and the initial phase detected was either in the downward (decrease) or in the upward (increase) direction in approximately equal frequency of occurrence (Fig. 7). Note that rapid swelling followed by contraction for squid giant axon (Iwasa and Tasaki 1980) and contraction followed by a slow swelling for a crayfish giant axon (Hill et al. 1977) have been reported with contact methods. In theory, a change in optical path length p may arise from changes in refractive index n and/or physical dimension d of the sample ($p = n \times d$). We monitored Δp between two fixed glass surfaces placed below and above the axon, but a refractive index–dependent change was not detected. The fact that the top surface of the axon alone showed changes in Δp in the nanometer range, whose magnitude is in good agreement with contact-mode measurements (Hill et al. 1977; Iwasa and Tasaki 1980), suggests our measurements can be attributed to physical changes within the axonal surfaces during AP propagation. In this case, the data shown in Fig. 7b suggest "local deformations," which puts in question Iwasa and Tasaki's (1980) statement identifying the swelling measured by their contact method to be the initial event in squid giant axons. By thinking of the event as a deformation, the direction could be impacted by deformations occurring in the adjoining regions of the observation point. A better understanding of these transient signals, if technology allows, may be obtained by simultaneously observing multiple depth profiles over an axon cross section and over the length of the axon, which may itself change during AP propagation.

The axon membrane thickness is ~7 nm. Surrounding the membrane is the Frankenhaeuser and Hodgkin (F-H) space with thickness of about 30 nm (Frankenhaeuser and Hodgkin 1956). Around the F-H space layer is the Schwann cell layer, which is 0.1–0.2 μm thick near the ends of the cells and 0.8–0.9 μm in the region of the nuclei; it is a dense layer (Villegas and Villegas 1960). Surrounding the Schwann cell layer is the basement membrane, which is a layer of low density with thickness of 0.1–0.2 μm. Outside the basement membrane there is an outer sheath approximately 20-μm-thick layer of connective tissue cells and

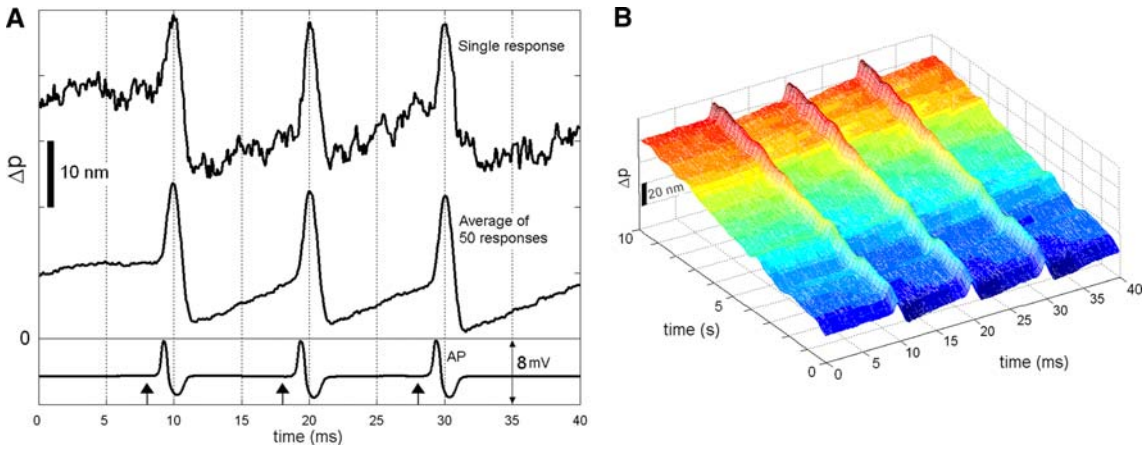

Fig. 8 A single and an average of 50 responses with the corresponding AP (**a**). A 21-nm peak-to-peak Δp between the top and bottom surfaces of the axon is obtained at cold temperature (~2°C) with 400 mM NaCl added to the seawater (*saline*). Three-dimensional plot (**b**) shows the progression of the fast signal over 10 s, and each trace along the fast time axis is a moving average of 10 records

collagen bundles (Bear et al. 1937). Since the axial resolution provided by our coherence function is about 4.3 μm in tissue, the phase signal can originate from one or more of these structures within the coherence volume, e.g., displacement of membrane and/or expansion or contraction of the F-H space. This may complicate interpretation of the signal as the system cannot resolve these submicron structures. More specifically, if there are stationary structures reflecting the light within the 4.3 μm depth range, the observed magnitude of deformation can be less than the actual magnitude. If the optical properties of structures within the 4.3 μm axial resolution somehow vary during activity (e.g., reflectivities change), the measurement may also be inaccurate. However, there is another possibility, that the region around the membrane (4.3 μm thick, 21 μm diameter) moves up or down; then, the observed Δp response will be highly accurate and representative for transient deformations. In our experiments we did find transient responses from points around and close to the peak of the coherence function, and the magnitude of the Δp repsonse was maximal at the peak. Furthermore, the literature reports 1-ms duration nanometer-scale transient deformations for single axons (Hill et al. 1977; Iwasa and Tasaki 1980), as observed here using our noncontact technique.

Hill (1950) suggested that swelling is partly due to the exchange of sodium and potassium across the membrane and partly due to transfer of sodium chloride into the fiber and accompanying water movement. The difference in hydration during sodium–potassium exchange and the entry of water molecules accompanying NaCl leads to an increase in osmotic pressure and subsequently swelling. The observed displacement is much larger than that expected by this mechanism of ion movements, and it is now known that very little chloride enters the axon (Landowne and Scruggs 1976). An increase in volume due to sodium ion movements is also discussed by Tasaki and Byrne (1990) and Kim et al. (2007). By assuming that displacement is caused by water accompanying sodium into the axon, our calculations show that for a 400-μm-diameter axon we need 138 water molecules for every sodium ion to obtain a change in diameter of 0.1 nm, assuming there is a movement of 4 pmole/cm^2/impulse of Na^+ ions during activity. The number 138 is very large when compared to the normal value of 3.2 (Hill 1950) or 2 (Kim et al. 2007) water molecules per sodium ion. Also, 138 water molecules per Na^+ ion is much more water than the 40–50 molecules/channel reported to associate with the average delayed rectifier potassium channel of the squid axon when it opens (Zimmerberg et al. 1990) because on the order of a few thousand ions pass through the open channel. However, some regions of the axon may be shrinking while other regions are swelling. Perhaps this could be explained by a nonuniform distribution of sodium channels (Almers et al. 1983; Gogan et al., 1995), although the magnitude of the transient deformations still seems too large to be explained by this mechanism.

We obtained mean values of optical path-length change (Δp response) to be 1.1 nm at room temperature (20–21°C) and 1.65 nm in cold (~2°C). Most of the Δp responses were <1.2 nm; for these the mean values at room temperature and in the cold were 0.57 and 0.68 nm, respectively. Thus, for most of our data, cooling increased the amplitude of the response by about 19%, which is close to the 18% increase in extra sodium influx associated with APs reported by Cohen and Landowne (1974). The 10% increase in AP amplitude seen by Hodgkin & Katz (1949) should also be noted. As a direct link between the sodium flux and the transient swelling (or shrinkage) seems tenuous, the physical change may be proportional to the change in membrane potential, perhaps by the converse flexoelectric effect discussed below.

The magnitude of the Δp response during AP propagation increased as the NaCl concentration in the seawater was increased (Fig. 5). Assuming the Δp response represents deformations, our findings with hypertonic solutions are in contrast to those of Tasaki and Iwasa (1982), who reported that a roughly 30% increase in tonicity, by the addition of sucrose, invariably reduced the amplitude of the mechanical response, which was measured with a stylus attached to a piezoelectric device. The effect of axon diameter may be studied further with increased levels of sucrose, which will shrink the axon but will not play a role like Na^+ during AP propagation. Our limited number of experiments with seawater and 133 mM additional calcium and 400 or 800 mM additional sucrose (data not shown) had an observable Δp response during activity.

Todorov et al. (1994) observed a converse flexoelectric effect (voltage-induced curvature strain) when a bilayer lipid membrane was subjected to 300 mV transmembrane AC potentials at frequencies ranging 100–450 Hz. Raphael et al. (2000) proposed that electrically induced localized changes in the curvature of the plasma membrane are responsible for the electromotility of outer hair cells. Petrov et al. (1989) suggested that at a negative sign of the flexoelectric coefficient and a negative transmembrane voltage the converse flexoelectric effect would act in the direction of decreasing the initial curvature of an Ω-shaped patch and may activate its direct flexoelectric response (curvature-induced electrical polarization) to an oscillating pressure difference. Also, Mosbacher et al. (1998) applied a ± 10 mV peak–peak AC carrier stimulus to voltage-clamped HEK293 cells and, using atomic force microscopy, reported that the cells moved 0.5–15 nm normal to the plane of the membrane. The converse flexoelectric effect may play a significant role for the transient signals

we recorded from the squid giant axon during AP propagation. This effect may be studied further, especially when axonal shrinkage (i.e., as a result of an increase in NaCl or sucrose concentration) alters the global as well as the local curvatures around the membrane. If the sign of the local membrane curvature changed with position, it might explain the variety of deformations.

Conclusion

Using noncontact phase measurements of an SD-OCT system, the magnitude and shape of the optical path-length changes recorded from squid giant axons during AP propagation are reported with statistics. Alterations in the magnitude and shape of these transient signals are reported at room and cold temperatures and with NaCl levels in the axon's environment. Also, progression of the fast signals with continuous stimulation is demonstrated to show the stability of the measurement and the repeatability of the fast response for a given location. The results range from subnanometers to 21 nm and were mostly biphasic. The initial direction of the response was the same for a single location, but opposite directions in approximately equal frequency of occurrence are observed for various locations. Therefore, the transient events appear to have local characteristics. We also reviewed and discussed a number of realistic and unrealistic mechanisms. Furthermore, our results may facilitate development of new theories on this matter.

Acknowledgements This work was supported by a research grant from the National Institutes of Health (EB006588, cofunded by NIBIB and NEI) and by the H. Keffer Hartline and Edward F. MacNichol, Jr. Fellowship Fund at the Marine Biological Laboratory (Woods Hole, MA).

References

Akkin T, Davé DP, Milner TE, Rylander HG III (2004) Detection of neural activity using phase-sensitive optical low-coherence reflectometry. Opt Express 12:2377–2386

Akkin T, Joo C, de Boer JF (2007) Depth-resolved measurement of transient structural changes during action potential propagation. Biophys J 93:1347–1353

Almers W, Stanfield PR, Stühmer W (1983) Lateral distribution of sodium and potassium channels in frog skeletal muscle: measurements with a patch-clamp technique. J Physiol 336:261–284

Bear RS, Schmitt FO, Young JZ (1937) The sheath components of the giant nerve fibres of the squid. Proc R Soc Lond B 123:496–504

Bryant SH, Tobias JM (1955) Optical and mechanical concomitants of activity in carcinus nerve I. Effect of sodium azide on the optical response II. Shortening of the nerve with activity. J Cell Comp Physiol 46:71–95

Cense B, Nassif NA, Chen T, Pierce M, Yun S, Park B, Bouma B, Guillermo T, de Boer JF (2004) Ultrahigh-resolution high-speed retinal imaging using spectral-domain optical coherence tomography. Opt Express 12:2435–2447

Choma MA, Ellerbee AK, Yang C, Creazzo TL, Izatt JA (2005) Spectral-domain phase microscopy. Opt Lett 30:1162–1164

Cohen LB (1973) Changes in neuron structure during action potential propagation and synaptic transmission. Physiol Rev 53:373–418

Cohen LB, Keynes RD, Hille B (1968) Light scattering and birefringence changes during nerve activity. Nature 218:438–441

Cohen LB, Hille B, Keynes RD (1969) Light scattering and birefringence changes during activity in the electric organ of electrophorus. J Physiol 203:489–509

Cohen LB, Hille B, Keynes RD (1970) Changes in axon birefringence during the action potential. J Physiol 211:495–515

Cohen LB, Landowne D (1974) The temperature dependence of the movement of sodium ions associated with nerve impulses. J Physiol 236:95–111

Fang-Yen C, Chu MC, Seung HS, Dasari RR, Feld MS (2004) Noncontact measurement of nerve displacement during action potential with a dual-beam low-coherence interferometer. Opt Lett 29:2028–2030

Fercher AF, Hitzenberger CK, Kamp G, Elzaiat SY (1995) Measurement of intraocular distances by backscattering spectral interferometry. Opt Commun 117:43–48

Frankenhaeuser B, Hodgkin AL (1956) The after-effects of impulses in the giant nerve fibres of *Loligo*. J Physiol 131:341–376

Gogan P, Schmiedel-Jakob I, Chitti Y, Tyc-Dumont S (1995) Fluorescence imaging of local membrane electric fields during the excitation of single neurons in culture. Biophys J 69:299–310

Hausler G, Lindner MW (1998) Coherence radar and spectral radar—new tools for dermatological diagnosis. J Biomed Opt 3:21–31

Hill BC, Schubert ED, Nokes MA, Michelson RP (1977) Laser interferometer measurement of changes in crayfish axon diameter concurrent with action potential. Science 196:426–428

Hill DK (1950) The volume change resulting from stimulation of a giant nerve fibre. J Physiol 111:304–327

Hill DK, Keynes RD (1949) Opacity changes in stimulated nerve. J Physiol 108:278–281

Hodgkin AL, Katz B (1949) The effect of temperature on the electrical activity of the giant axon of the squid. J Physiol 109:240–249

Huang D, Swanson EA, Lin CP, Schuman JS, Stinson WG, Chang W, Hee MR, Flotte T, Gregory K, Puliafito CA, Fujimoto JG (1991) Optical coherence tomography. Science 254:1178–1181

Iwasa K, Tasaki I (1980) Mechanical changes in squid giant axons associated with production of action potentials. Biochem Biophys Res Commun 95:1328–1331

Joo C, Akkin T, Cense B, Park BH, de Boer JF (2005) Spectral-domain optical coherence phase microscopy for quantitative phase-contrast imaging. Opt Lett 30:2131–2133

Kim GH, Kosterin P, Obaid AL, Salzberg BM (2007) A mechanical spike accompanies the action potential in mammalian nerve terminals. Biophys J 92:3122–3129

Landowne D, Scruggs V (1976) The temperature dependence of the movement of potassium and chloride ions associated with nerve impulses. J Physiol 259:145–158

Mosbacher J, Langer M, Hörber JKH, Sachs F (1998) Voltage-dependent membrane displacements measured by atomic force microscopy. J Gen Physiol 111:65–74

Nassif N, Cense B, Park BH, Yun SH, Chen TC, Bouma BE, Tearney GJ, de Boer JF (2004) In vivo human retinal imaging by ultrahigh-speed spectral domain optical coherence tomography. Opt Lett 29:480–482

Park BH, Pierce MC, Cense B, Yun SH, Mujat M, Tearney GJ, Bouma BE, de Boer JF (2005) Real-time fiber-based multi-functional spectral-domain optical coherence tomography at 1.3 μm. Opt Express 13:3931–3944

Petrov AG, Ramsey RL, Usherwood PNR (1989) Curvature-electric effects in artificial and natural membranes studied using patch-clamp techniques. Eur Biophys J 17:13–17

Raphael RM, Popel AS, Brownell WE (2000) A membrane bending model of outer hair cell electromotility. Biophys J 78:2844–2862

Sivaprakasam A, Landowne D, Akkin T (2008) Non-contact optical measurement of nanometer range deformations in squid giant axon structure during activity. Biophys J 94:817

Tasaki I, Watanabe A, Sandlin R, Carnay L (1968) Changes in fluorescence, turbidity, and birefringence associated with nerve excitation. Proc Natl Acad Sci USA 61:883–888

Tasaki I, Iwasa K (1982) Rapid pressure changes and surface displacements in the squid giant axon associated with production of action potentials. Jpn J Physiol 32:69–81

Tasaki I, Kusano K, Byrne PM (1989) Rapid mechanical and thermal changes in the garfish olfactory nerve associated with a propagated impulse. Biophys J 55:1033–1040

Tasaki I, Byrne PM (1990) Volume expansion of nonmyelinated nerve fibers during impulse conduction. Biophys J 57:633–635

Todorov AT, Petrov AG, Fendler JH (1994) First observation of the converse flexoelectric effect in bilayer lipid membranes. J Phys Chem 98:3076–3079

Tripathi R, Nassif N, Nelson JS, Park BH, de Boer JF (2002) Spectral shaping for non-gaussian source spectra in optical coherence tomography. Opt Lett 27:406–408

Villegas GM, Villegas R (1960) The ultrastructure of the giant nerve fibre of the squid: axon–schwann cell relationship. J Ultrastruct Res 3:362–373

von Muralt A (1975) The optical spike. Philos Trans R Soc Lond B Biol Sci 270:411–423

White BR, Pierce MC, Nassif N, Cense B, Park BH, Tearney GJ, Bouma BE, Chen TC, de Boer JF (2003) In vivo dynamic human retinal blood flow imaging using ultra-high-speed spectral domain optical Doppler tomography. Opt Express 11:3490–3497

Wojtkowski M, Leitgeb R, Kowalczyk A, Fercher AF (2002) Fourier domain OCT imaging of the human eye in vivo. Proc Soc Photo Opt Instrum Eng 4619:230–236

Yao X, Rector DM, George JS (2003) Optical lever recording of displacements from activated lobster nerve bundles and *Nitella* internodes. Appl Opt 42:2972–2978

Yazdanfar S, Yang C, Sarunic MV, Izatt JA (2005) Frequency estimation precision in Doppler optical coherence tomography using the Cramer-Rao lower bound. Opt Express 13:410–416

Zimmerberg J, Bezanilla F, Parsegian VA (1990) Solute inaccessible aqueous volume changes during opening of the potassium channel of the squid giant axon. Biophys J 57:1049–1064